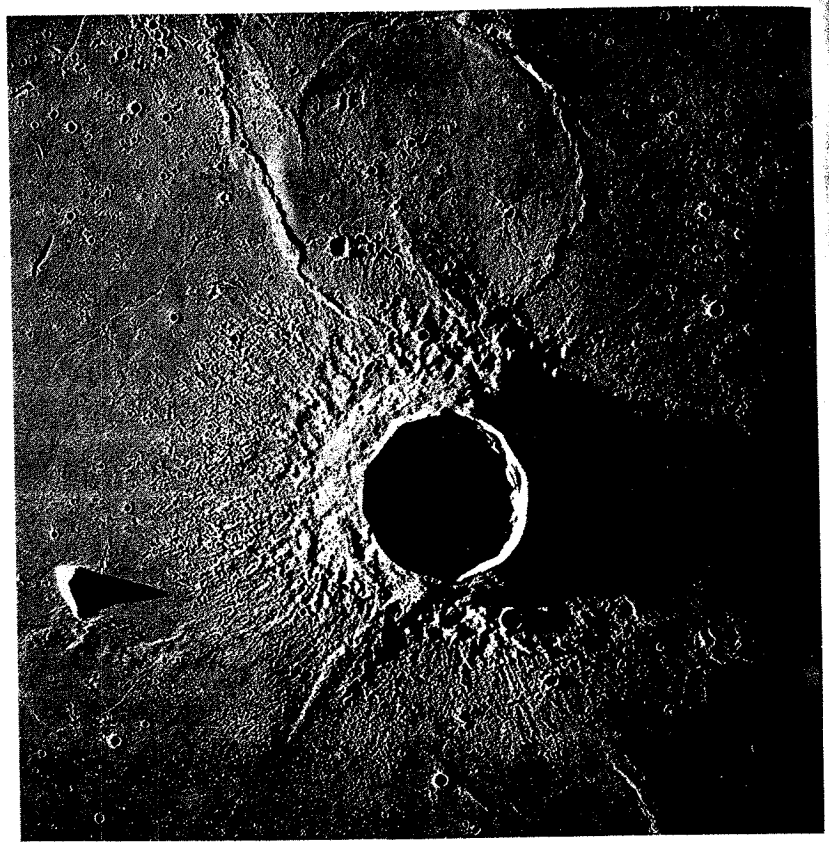

A photograph of the lunar crater Lambert ($\lambda = 21°$ W, $\beta = 26°$ N) and its 'ghost' companion (Lambert *R*), taken by the metric camera (Frame No. 1011) of the Apollo 15 mission in August 1971. (South is on top, West to the right).

(Reproduced by courtesy of NASA.)

THE MAPPING OF LUNAR RADAR SCATTERING CHARACTERISTICS

G. H. PETTENGILL* and S. H. ZISK

Haystack Observatory, Massachusetts Institute of Technology, Westford, Mass., U.S.A.

and

T. W. THOMPSON**

Arecibo Observatory, Arecibo, Puerto Rico, U.S.A.

(Received 30 June, 1973)

Abstract. This is the first of four articles describing a comprehensive series of radar maps of the entire visible lunar hemisphere carried out at wavelengths of 3.8 and 70 cm and analyzing the echoes in both orthogonal senses of circular polarization. In this paper, the basic techniques of delay-Doppler mapping by radar are developed, and the particular steps employed in mapping the Moon are outlined. Succeeding articles present the results obtained and discuss the way in which these results relate to other, nonradar measurements as well as to the actual lunar surface properties.

1. Introduction

Observations of the Moon by radar, made shortly before the beginning of this decade (Pettengill, 1960; Leadabrand *et al.*, 1960), established the presence of a diffusely scattered echo component, which was interpreted as originating in wavelength-sized lunar surface structure. This conclusion was reinforced by later investigations using a variety of observing wavelengths and polarizations. Particularly significant was the discovery of anomalously strong scattering from the region of the crater Tycho (Pettengill and Henry, 1962), which was most easily accounted for on the assumption of a local increase in the amount of wavelength-sized surface roughness, a finding which has been subsequently verified (Pettengill and Thompson, 1968). Ground-based telescopic observations of the Moon, even under the best conditions of optical seeing, have yielded resolution of the lunar surface of no better than a few hundred meters. Orbital and surface photography has provided information on surface structure of the order of a meter in size, but only at considerable expense. Therefore, optical coverage at this high resolution has been limited to a relatively few selected areas. Since the diffusely scattered component of the radar echo has been shown to be directly related to the distribution of wavelength-sized irregularities across the lunar surface, its measurement at centimeter and decimeter wavelengths provides a comparatively inexpensive assessment of the local surface roughness in a size range of interest in many lunar surface studies, including those preparatory to a selection of lunar landing sites.

* Now at the Department of Earth and Planetary Sciences, Massachusetts Institute of Technology, Cambridge, Mass., 02139, U.S.A.

** Now at the Jet Propulsion Laboratory, California Institute of Technology, Pasadena, Calif., 91103, U.S.A.

The Moon **10** (1974) 3–16.

With this application in mind, the U.S. National Aeronautics and Space Administration has supported several series of radar mapping studies of the Moon, both at the Arecibo Observatory in Puerto Rico and at the Haystack Observatory in Massachusetts. It is our intent to present the major results from these studies in a series of four papers. In the present paper, a discussion of the technique will be given as background for the more detailed papers to follow.* The second and third papers will present the Arecibo (70-cm wavelength) and Haystack (3.8 cm wavelength) results, respectively, while the fourth will intercompare the results at the two wavelengths. From the variations among the different observations, it should prove possible to deduce the surface distribution of wavelength-sized irregularities, as well as to locate regions having atypical local surface slopes.

2. Delay-Doppler Mapping Technique

Unlike the situation at optical wavelengths, where angular resolution of better than 1″ can readily be obtained (even with small telescopes), straightforward attempts at angular resolution using currently available antenna beamwidths are limited to about 4′ at radar wavelengths. While affording some resolution of the 30′-diam lunar disk, this level of resolution does not permit fine-grained comparison between radar and optical scattering characteristics in localized areas of the lunar surface.

One could conceive of an interferometric observing system which would offer resolution approaching a few seconds of arc; because of the complex source distribution represented by the lunar disk, however, a large number of effective baselines (spatial Fourier components) would be required to determine the distribution unambiguously.

As a rigid body, the Moon maintains an exact positional relationship among its surface features. Thus a known motion of the whole body implies a predictable motion for each of its components. For example, because of the apparent lunar rotation as viewed from the radar, there will be a calculable locus of surface points which possess the same Doppler-shifted echo frequency. Thus, frequency analysis with adequate resolution will select that component of the echo which originates from a known strip on the lunar surface.

An alternative way of looking at this phenomenon is to visualize the wavefront of the echo as it arrives at the surface of the Earth. Since all elements of the lunar scattering surface are maintaining their relative alignment, rotation of the Moon will serve only to sweep a fixed wavefront pattern past the antenna. Thus, sequential sampling of the received signal is equivalent to a simultaneous sampling of the original waveform over the dimension swept out by the antenna during the time interval of observation. In this way, one uses the coherence in time of the echo wavefront to synthesize a very much larger aperture than is available for simultaneous observation and thus to obtain a vastly improved effective angular resolution. In the radar case, of course,

* Somewhat different techniques have produced radar maps of the Moon at wavelengths of 23 cm (Hagfors *et al.*, 1968), 74 cm (Thomson and Ponsonby, 1968), and 7.5 m (Thompson, 1971).

the location of the illuminating wave front with respect to the lunar surface is also being varied with time. To first order, however, this merely doubles the apparent motion of the antenna through a hypothetical scattered wavefront fixed to the Moon.

If the distribution of echo power in delay is measured simultaneously with this frequency distribution, a mapping of the echo power across the lunar surface is possible as shown in Figure 1. A convenient Cartesian coordinate system in which to express these measurements is defined by the direction cosines x, y, and z, with the origin at the lunar center of mass, where z is directed toward the radar, y is directed at right angles to z in the plane containing z and the apparent axis of rotation, and x is

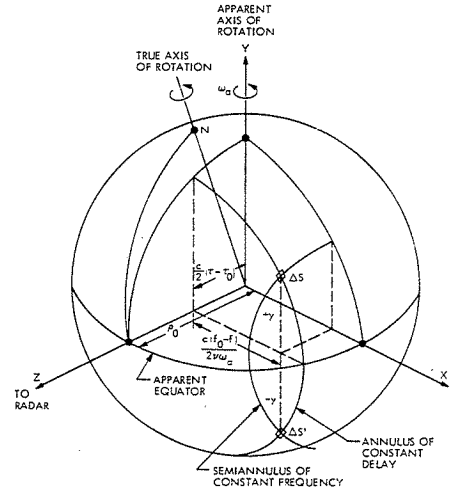

Fig. 1. Definition of delay-Doppler mapping coordinates x, y, z. The two ambiguous scattering areas are ΔS and $\Delta S'$. The scattering areas are very small fractions (10^{-5} or less) of the total visible surface.

chosen to complete a righthanded orthogonal set. In terms of the measured delay τ and Doppler shift f, the (dimensioned) coordinates are given by

$$X = c(f_0 - f)/2\nu\omega_a = \lambda(f_0 - f)/2\omega_a \quad (1)$$

$$Z = c(\tau_0 - \tau)/2 \quad (2)$$

where τ_0 and f_0 are the delay and Doppler shift corresponding to the lunar center of mass, c is the velocity of light, ν is the radar carrier frequency, λ is radar wavelength, and ω_a is the apparent lunar rotation projected in the x-y plane. In the absence of any further information about the echo, a projection in the x-y plane is all that can be obtained, just as in the case of optical mapping where only the projection in the x-y plane is directly yielded.

If we let ϱ be the radius (which may vary by a few parts per 1000 over the surface,

of course) between the surface 'point' responsible for the echo and the lunar center of mass, then the direction cosines for points on the surface become

$$x = X/\varrho = c(f_0 - f)/2\varrho v\omega_a \tag{3}$$

$$z = Z/\varrho = c(\tau_0 - \tau)/2\varrho \tag{4}$$

$$y = \pm (1 - x^2 - z^2)^{1/2} \tag{5}$$

where the two branches of y reflect an actual ambiguity as may be seen from Figure 1.

In order to proceed further with the mapping, it is necessary to find a means of isolating the two branches of Equation (5). This is done in the present case by selecting only those echoing areas for which the angular separation of the ambiguous regions $(4y\varrho/c\tau_0)$ is greater than the angular half-power beamwidth of the radar antenna. Assuming that this has been accomplished, the analysis reduces to a reconstruction onto a near-spherical surface from a projection in the x-z plane. Because the topographic deviations of the surface are small, we shall assume a sphere of constant radius ϱ_0.

Furthermore, since we wish to refer the observed scattered power density $P(x, z)$ to unit area on the (assumed spherical) lunar surface, the Jacobian of the transformation from the x-z plane to this surface must be calculated to yield

$$P'\Delta s = P|y|\,\Delta x \Delta z \tag{6}$$

where P' is the desired density per unit area of the surface. Strictly speaking, Equation (6) holds only for truly differential areas, whereas radar measurements have finite

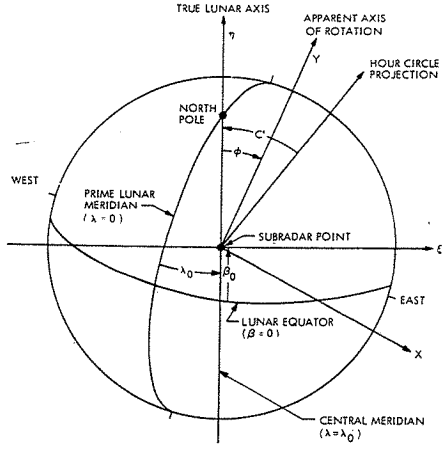

Fig. 2. The Moon's disk showing the angles and coordinates used in calculating radar ephemerides. Angle ϕ is the Doppler angle (Equations (7) and (8); angle C' is the position angle of the optical axis; λ and β are lunar latitude and longitude; λ_0 and β_0 are the lunar latitude and longitude of the subradar point. Radar coordinates are x and y (Equations (3), (4), and (5) and Figure 1); observer coordinates are ξ and η. The hour angle projection lies along the celestial right ascension of the center of the disk.

resolution in delay and Doppler. However, the mapping reported here is carried out under conditions where the use of the differential limit leads to no significant error.

Following this modification to the observed power, three coordinate rotations are required to locate the observed density in terms of standard selenographic coordinates. First, one seeks the transformation from the x, y, z system (the 'radar' coordinates) to the ξ, η, z system (the 'observer' coordinates), where η is the direction of the lunar north pole projected in the x-y plane and ξ completes a right-handed Cartesian coordinate system (Figure 2):

$$\begin{aligned} \xi &= x\cos\phi + y\sin\phi \\ \eta &= -x\sin\phi + y\cos\phi; \end{aligned} \tag{7}$$

with its inverse

$$\begin{aligned} x &= \xi\cos\phi - \eta\sin\phi \\ y &= \xi\sin\phi + \eta\cos\phi. \end{aligned} \tag{8}$$

The angle ϕ (the Doppler angle) is measured positively in the clockwise direction from the lunar meridian passing through the subradar point to the great circle arc connecting the subradar point and the positive direction of the apparent rotation vector (see Figure 2).

After the rotations described above, the remaining transformations are those used in determining lunar coordinates from (Earth-based) optical photographs of the Moon (see, for example, Arthur, 1963). Thus two rotations are necessary to transform from the system of observer coordinates centered on the subradar point to the standard Cartesian selenographic grid aligned with the lunar equator and prime meridian

$$\begin{aligned} x_s &= \cos\beta\sin\lambda = \xi\cos\lambda_0 - \eta\sin\beta_0\sin\lambda_0 + z\cos\beta_0\sin\lambda_0 \\ y_s &= \sin\beta = \eta\cos\beta_0 + z\sin\beta_0 \\ z_s &= \cos\beta\cos\lambda = -\xi\sin\lambda_0 - \eta\sin\beta_0\cos\lambda_0 + z\cos\beta_0\cos\lambda_0 \end{aligned} \tag{9}$$

where

$$\beta = \arcsin(y_s), \qquad \lambda = \arctan(x_s/z_s) \tag{10}$$

are the usual selenographic latitude β and longitude λ and where β_0 and λ_0 are the corresponding coordinates of the subradar point. A useful inverse relation is

$$\begin{aligned} \xi &= \cos\beta\sin(\lambda - \lambda_0) \\ \eta &= \sin\beta\cos\beta_0 - \cos\beta\sin\beta_0\cos(\lambda - \lambda_0). \end{aligned} \tag{11}$$

Thus the observed reflected power density may be related to the specific scattering of an element of area on the lunar surface through Equations (6), (7), and (9).

The area resolution ΔS of the lunar surface resulting from a choice of pulse width $\Delta\tau$ and frequency filter width Δf is derived in Appendix A and is given by

$$\Delta S = \frac{c^2}{4v\omega_a}\frac{\Delta\tau\Delta f}{|y|} \tag{12}$$

where the constants are as defined previously and y may be obtained from Equations (8) and (11). The shape of ΔS will vary depending upon its location on the Moon as described in Appendix A.

In defining the radar coordinate system, it was assumed that the radar line of sight remained parallel over the surface of the Moon, i.e., that parallax was negligible. This is, of course, not quite true, since the lunar disk subtends about 0.5 deg at the radar. Because the relatively small antenna beamwidths used in the work reported here localized the area mapped in a given observation, it was permissible, to the accuracy preserved in the mapping, to assume that the amount of parallax remained constant over a given map. The effect of parallax is included, however, in the ephemeris calculation relating to the position of the center of the mapped area.

A major advantage of the delay-Doppler mapping method lies in its extremely high potential for resolution. This is due in part to the fact that modern radars are not signal-limited in viewing the Moon. Thus the delay and Doppler resolutions are restricted almost entirely by system stability and data processing constraints. Because the apparent lunar rotation is relatively slow, the Doppler spread across the region illuminated by the radar beam, even at high microwave frequencies, is smaller than the reciprocal of the delay spread across the same region. Thus aliasing resulting from constraints on the repetitive sampling of a given region can be avoided simultaneously in both delay and Doppler. The Doppler resolution may be made arbitrarily small (at least to the point where oscillator stability and atmospheric propagation limitations enter) by increasing the interval over which coherent observations are made. For a given total duration of observations, however, increasing this interval will correspondingly reduce the total number of such coherent intervals. The accuracy of the estimate of the mean of the fluctuating scattering to be identified with a given lunar surface element depends on the square root of the number of these independent intervals. Thus, increasing the Doppler resolution will automatically degrade the intensity resolution. Nevertheless, in respect to the product of these resolutions, the delay-Doppler method offers quite acceptable results in those areas of the surface where the radar coordinate y (see Equation (12)) is not unreasonably small.

Because the Doppler angle ϕ for the Moon can vary from -180 to 180 deg, judicious selection of observing times permits all portions of the lunar surface to be mapped under conditions where y will be relatively large. An exception is the region near the center of the lunar disk. Here, however, libration offers relief, since this awkward region will migrate sufficiently during the course of a month to permit even regions of low latitude and longitude to be mapped with adequate resolution.

3. Ephemeris

To enable mapping by radar, a number of quantities concerning the location and orientation of the Moon must be calculated. As input, the standard astronomical quantities as tabulated in the American Ephemeris and Nautical Almanac (United States Naval Observatory, 1965) have been assumed except where noted. These

exceptions are values for the horizontal parallax and the geocentric right ascension and declination obtained from an improved lunar ephemeris supplied by the Jet Propulsion Laboratory (Mulholland and Block, 1967).

These calculations separate naturally into two parts. The first is directed to the problem of deriving the absolute time of flight and Doppler shift for transmissions from the radar to the lunar center of mass. The second obtains the displacements in those parameters which are associated with locations on the surface. In the present circumstances, these ephemeris predictions are based on a relative accuracy requirement of 500 m in distance (equivalent to about 3μs in round-trip time delay) and a relative accuracy requirement of 1 mm s^{-1} in the component of velocity along the radar line of sight (equivalent to about 0.05 Hz at the 3.8 cm wavelength). Since the absolute values corresponding to the lunar subradar point were measured at intervals during the observing period, equivalent precision in the absolute delay and Doppler was not required, although in some cases it was found necessary to correct for known effects of topography in the vicinity of the subradar point in order to achieve the desired precision in absolute delay and Doppler.

The requirements for angular tracking of the antenna beam are less severe. With a two-way, half-power beamwidth of 4′ at 3.8 cm, a calculated angular precision of 0.1′ (about one-half the error contributed by the Haystack antenna control system) was thoroughly adequate. This error is equivalent to about 10 km when referred to the lunar surface. Even coarser tracking could be tolerated for the 8′ beam used in the 70-cm observations at the Arecibo Observatory.

The topocentric position of the Moon is obtained from the tabulated geocentric positions and orientations using standard equations (e.g., Arthur, 1963). In addition to the apparent right ascension, declination, and distance of the Moon's center, the position angle of the lunar axis and the selenographic coordinates of the subradar point are desired.

We now attack the problem of deriving the distance D and its time rate of change $\dot{D}$ for any arbitrary point on the lunar surface, given the distance to the center R and its rate of change $\dot{R}$. The geometry of the radar and lunar surface in the ξ, η, z (ob-

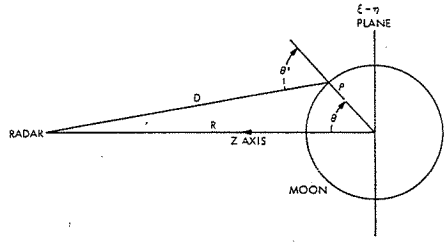

Fig. 3. Geometry for computation of distance D between radar and a point on the lunar surface. The size of the Moon is greatly exaggerated since the Earth-based radar will be about 240 lunar radii from the center of the Moon. Note that angle of incidence of radar beam θ' cannot differ from parallel-ray approximation θ by more than the angular radius of the Moon, approximately 0.25 deg.

server) coordinate system is shown in Figure 3. Here the radar is on the z-axis at a distance R from the center of the Moon. The point on the lunar surface has been placed in the plane of the paper. The distance D to this point is given by the law of cosines as

$$D = (R^2 + \varrho^2 - 2\varrho R\cos\theta)^{1/2} = (R^2 + \varrho^2 - 2\varrho z R)^{1/2} \tag{13}$$

where z is the coordinate of the surface point as defined in Equation (4). The time derivative of D is

$$\dot{D} = \frac{1}{D}[(R - \varrho z)\,\dot{R} - \varrho R\dot{z}]. \tag{14}$$

The distance and its time derivative are related to the echo roundtrip delay τ and Doppler frequency f (to second order in $\dot{D}$) by

$$\tau = \frac{2}{c}D \tag{15}$$

$$f = -\frac{2\nu\dot{D}}{c}\left(1 - \frac{\dot{D}}{2c}\right) \tag{16}$$

where c is the velocity of light, ν is the radar carrier frequency, and D and its derivatives are calculated at the instant of reflection ($\tau/2$ later than transmission, $\tau/2$ earlier than reception).

In Equation (14), the term in $\dot{R}$ accounts for the motion of the center of the Moon with respect to the radar, while the additional factor $(R-\varrho z)/D$ corrects for the parallax. The term in $\dot{z}$ arises from the apparent rotation of the Moon with respect to the radar. The apparent motion of the Moon results in part from the changing parallax of the observer as the Earth rotates and in part from the changing geocentric libration. Thus the selenographic coordinates β_0 and λ_0 of the subradar point are constantly changing.

Differentiation of z yields

$$\dot{z} = \eta\dot{\beta}_0 + \xi\cos\beta_0\dot{\lambda}_0. \tag{17}$$

The term in $\dot{\beta}_0$ describes the apparent rotation about the ξ-axis, and the term in $\dot{\lambda}_0$ about the η-axis. (The rotation about the z-axis does not induce a velocity component toward the radar.) The total apparent rotation thus has a magnitude ω_a and lies in the ξ-η plane at the angle ϕ from the selenographic meridian of the sub-radar point (see Figure 2). These quantities are derived from Equation (17) as

$$\phi = \arctan\left(\frac{-\dot{\beta}_0}{\dot{\lambda}_0\cos\beta_0}\right) \tag{18}$$

$$\omega_a = (\dot{\beta}_0^2 + \dot{\lambda}_0^2\cos^2\beta_0)^{1/2}. \tag{19}$$

The signs in the argument of the arctangent were chosen in agreement with the definitions for ϕ shown in Figure 2. Equation (17) may be rewritten as

$$\dot{z} = \omega_a(-\xi\cos\phi + \eta\sin\phi) = -\omega_a x \tag{20}$$

where the latter follows from Equation (8).

The calculation of the time delay τ and Doppler shift f to an arbitrary point on the lunar surface specified in selenographic coordinates may now be performed through successive applications of Equations (11), (18), (19), and (20), it being recalled that

$$z = (1 - \xi^2 - \eta^2)^{1/2} \tag{21}$$

and Equations (13) through (16). The epoch for these calculations is the instant of reflection from the lunar surface. If it is desirable to relate τ and f to the instant of transmission or reception, the epoch may be shifted appropriately by $\tau/2$.

In order to properly aim the antenna, it is necessary to find the apparent right ascension and declination of the desired map area on the lunar surface. First the right ascension and declination of the center of the Moon are found, using the tabulated geocentric values with standard topocentric corrections. Then the offset in these coordinates is determined for the desired position on the lunar surface.

As viewed from the radar, the Moon subtends a small angle, so that the contours of right ascension and declination projected onto the lunar disk form a nearly orthogonal grid. In fact, in this projection the two contours depart from orthogonality by no more than 2″. The orientation of these contours with respect to the ξ and η axes is given by C', the position angle of the optical axis, as defined in Figure 2. The differences in topocentric right ascension $\Delta\alpha$ and declination $\Delta\delta$, measured from the center of the lunar disk, are determined by a rotation of the ξ–η plane about the z-axis through the angle C'. Thus,

$$\begin{aligned}\Delta\alpha &= [\xi\cos(C') - \eta\sin(C')]\,s\cos(\delta')\\ \Delta\delta &= [\xi\sin(C') + \eta\cos(C')]\,s\end{aligned} \tag{22}$$

where s = angular semidiameter of the Moon = $\arctan(\varrho/R)$,
and δ' = topocentric declination of the Moon's center of mass.

4. Observing and Data Reduction Procedures

There were five main steps in the production of the radar maps of the Moon presented in the succeeding articles: (1) preparing for a run, (2) making observations, (3) spectrum analysis, (4) computer mapping, and (5) display. Since many of the operating constraints and parameters differed between the two sets of observations (at 70 and 3.8 cm), only a general description is given here.

Preparation for a run involved selection of observing time such that the lunar libration and the position angle of the apparent axis of rotation were appropriate for mapping the desired areas of the Moon. This was done with the help of a special

ephemeris program which, for a specified time, delineated the regions where the angular resolution of the antenna would ensure freedom from mapping ambiguity. This ephemeris program also gave surface resolution assuming standard values of delay and frequency resolution. In this way an observer could plan his schedule so as to record data for each region of the Moon at the optimum time. Careful planning was particularly necessary for observation of the equatorial regions because of the limited period during each month when the apparent axis lay farthest from the true axis and when the mapping of these regions could thus best be carried out.

Observations were broken into individual runs with a duration set by the need to achieve specified levels of statistical accuracy in the estimation of mean echo strength or by constraints in the observing geometry, whichever was reached first. The size of the region of the lunar surface which could be mapped during a given run was determined either by the 'footprint' of the antenna beam (for areas nearer the subradar point) or by limitations in the number of delay samples which could be stored in the data taking program (for areas nearer the limb). During the observations, the antenna was steered by computer to track the center of the region being mapped. Circularly polarized pulses of a length compatible with the desired resolution were transmitted at an interval large in comparison with the total delay spread corresponding to the lunar radius (11.6 ms). Thus there was no possibility of confusing echoes from the wrong delay.

The precise value of interpulse period was chosen so that the desired portion of the returned lunar echo always fell in a part of the interpulse well separated from a neighboring transmitter pulse. During the period of reception, the receiving local oscillator was automatically adjusted many times a second (maintaining phase continuity) to compensate for the varying Doppler shift corresponding to echoes from the center of the region under observation. Similarly, the sampling in delay was continuously adjusted to compensate for the changing echo delay. In this way, subsequent data processing had to contend only with second-order effects in delay and Doppler correction.

A pair of phase-sensitive, synchronous detectors were used in phase quadrature for each of the two orthogonal, circularly polarized senses of received polarization. In this way, full spectral information was preserved over a band equal to the pulse repetition frequency. The pulse repetition frequency was chosen (subject also to the constraints listed previously) so that it always exceeded the Doppler spread of the area illuminated by the antenna. The outputs of the four detectors (two for each polarization sense) were sampled simultaneously at intervals corresponding to the transmitted pulsewidth, converted into 8-bit digital words, and transferred into a CDC-3300 digital computer for temporary storage on magnetic tape. An estimate of the background, no-target receiver noise level was obtained either by sampling a portion of the interpulse interval where no echo was present (at 3.8 cm) or by frequency-analyzing a portion of the spectral window where no echo was present (at 70 cm).

The sense of circular received polarization corresponding to that transmitted is

called the depolarized mode, since only those elements of the lunar surface which scatter incoherently will contribute to this received component. The orthogonal sense is called the polarized mode and contains the bulk of the echo power returned by the Moon. In many other radar reports, the polarized mode is often referred to as the 'expected' mode. A more complete discussion on how the relative echo strengths of the two modes can be used to deduce local properties of the lunar surface is given by Thompson and Zisk (1972).

Following the actual observations, the echo time sequences are Fourier-analyzed, using a Cooley-Tukey algorithm. The series of phase-quadrature records from corresponding samples of successive interpulse intervals thus yield, in the transform, an estimate of the echo power distribution in frequency at a given delay. The resolution is set by the length of the series used in the transform, while the statistical accuracy of the estimate of echo intensity depends on the number of such series in the total set. It can readily be seen that frequency resolution and statistical accuracy are in direct conflict for a run of fixed duration. In general, between 50 and 100 coherent integration periods (CIP's) were found to yield an acceptable accuracy in intensity, while the frequency resolution required varied between 0.01 and 0.1 Hz. The frequency-analysis step in the data reduction required by far the largest fraction of total computer time allocated to producing the lunar maps. Following the frequency analysis of each CIP, the results were squared (to obtain power) and stored on magnetic tape to yield a series of matrices (one for each CIP) of received echo power as a function of delay and Doppler. These matrices serve as input to the mapping step of data reduction.

The mapping program has the task of applying corrections to the raw received power and then identifying and summing those elements of the observed power which correspond to each resolved element in the desired output map. The corrections applied to the data are (1) subtraction of noise background (determined independently as described above), (2) normalization to account for possible variations in radar system parameters such as transmitter power and receiver bandwidth, (3) allowance for the effects of finite antenna beamwidth, (4) normalization to the mean lunar scattering law characteristic of the wavelength and mode of polarization used, and (5) normalization to account for the Jacobian of the coordinate transformation (as given in Equation 6). The normalization to the mean lunar scattering is useful, since it emphasizes local departure from average behavior. In addition, it reduces the enormous dynamic range (about a factor of 1000 in power) which would otherwise exist between echoes from near the subradar point and from the lunar limb.

Since the sampling of the radar waveform occurs at discrete intervals, the mapping transformation is similarly discrete. But because the transformation is changing with time during the course of a run (primarily through changes in the apparent rotation ω_a and in the Doppler angle ϕ), the mapped result appears relatively smooth in most cases, even though the surface resolution must reflect the basic input sampling interval in delay and frequency.

The mapping program has access to the necessary ephemeris data, and as it reads

the radar data it calculates into which element of the final map that datum should be placed (after the corrections described above). A check is also made to assure that sufficient rejection of echo power associated with the ambiguous (conjugate) hemisphere exists. The map may be produced or reprojected in either Mercator, Lambert conformal, or orthographic projections. Following the calculations described above, the numerical data are displayed in analog form on an oscilloscope and photographed (as described in somewhat greater detail in the next articles).

5. Summary

In this article, we have reviewed in some detail the methods and mathematics employed in the delay-Doppler mapping of lunar surface radar scattering. Subsequent articles which present detailed results obtained at wavelengths of 3.8 and 70 cm will draw on this material as an introduction and reference.

As a technique for mapping distant planetary surfaces with high resolution, delay-Doppler radar resolution offers distinct advantages. Unlike Earth-based optical study, the method does not suffer degradation with distance as a result of basic limitations in the Earth's atmosphere. Given the requisite radar sensitivity, the surface of Venus, or even Titan, can be mapped to a resolution of a few kilometers or better with an Earth-based radar. And, of course, radar has the ability to penetrate the persistent cloud cover of Venus.

Acknowledgments

The radar measurements at both the Haystack and Arecibo Observatories were supported by NASA under Contract NAS 9-7830 and by NASA Grant 33-010-024, respectively.

Appendix A

Size and Shape of Radar Resolution Cell

This appendix describes the size and shape of the radar resolution cell, the area resolved by a single measurement in both delay and frequency. It is convenient to consider the two projections of the Moon's surface shown in Figure A-1. The terms annuli will describe the area resolved by a single delay or frequency measurement. Figure A-1 shows the Moon as observed from a point on the apparent axis of rotation and where both the delay and frequency annuli are viewed edge-on. Figure A-1a shows the Moon as viewed from the radar. The coordinates X, Y, Z are the radar coordinates described by Equations (3), (4), and (5) of the text.

The shape of the radar resolution cell, as indicated in Figure A-1, is a parallelogram on the surface of the Moon. Generally, the radar maps are made of areas which are near the apparent axis of rotation when projected into the X-Y plane as shown in Figure A-1b. Thus, the resolution cell will be nearly rectangular (but very rarely square).

The size of the radar resolution cell is easily approximated. The size of this cell

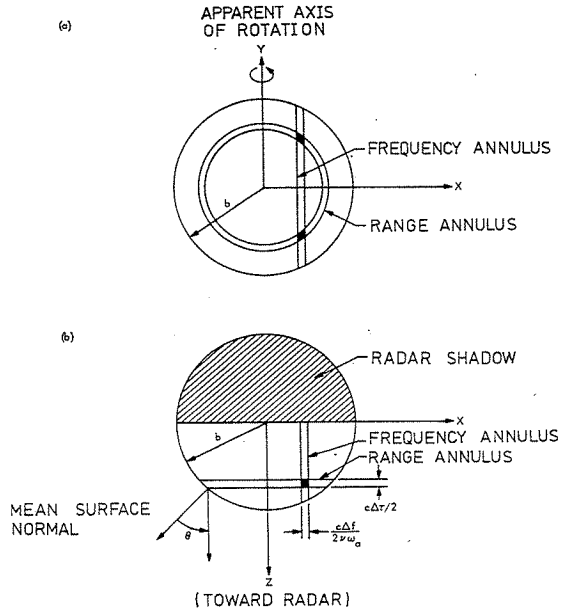

Fig. A-1. The Moon and representative delay and frequency annuli in the radar coordinates (a) the Moon as seen by the radar with z out of plane of the paper, and (b) the Moon as viewed from the rotation pole with y out of the paper. The angle of incidence θ is the angle between the mean surface normal and the direction of the radar. It should be noted that the radar's resolution $c\Delta\tau/2$ and $c\Delta f/2v\omega_a$ are very small fractions (a few thousandths) of the lunar radius.

when projected into the X-Z plane (as shown in Figure A-1b) is

$$\Delta S_{\text{projected}} = \Delta X \Delta Z = \left(\frac{c\Delta f}{2v\omega_a}\right)\left(\frac{c\Delta\tau}{2}\right) \tag{A-1}$$

where ΔX is the edge-on width of the frequency annulus, ΔZ is the edge-on width of the range annulus, c is the velocity of light, v is the radar's frequency, ω_a is the apparent rotation rate of the Moon, and where Δt and Δf are the delay and frequency resolutions of the measurement. One notes that

$$\begin{aligned} &\mathbf{n} = \text{vector normal to the surface} = x\mathbf{u}_x + y\mathbf{u}_y + z\mathbf{u}_z \\ &\mathbf{o} = \text{unit vector in the direction of projection} = \mathbf{u}_y . \end{aligned} \tag{A-2}$$

The terms $\mathbf{u}_x$, $\mathbf{u}_y$, and $\mathbf{u}_z$ are unit vectors along the principal axes of the x, y, z coordinate system. Thus p, the angle between the surface normal at the resolution cell and the unit vector in the direction of projection, is given by

$$\cos(p) = \mathbf{n}\cdot\mathbf{o} = |y| . \tag{A-3}$$

The size of the radar resolution cell on the surface, ΔS, is given by

$$\Delta S = \frac{c^2}{4v\omega_a} \frac{\Delta\tau\Delta f}{|y|} \tag{A-4}$$

which is Equation (12) in the text.

References

Arthur, D. W. G.: 1963, in *Moon, Meteorites and Comets*, Vol. IV of The Solar System, University of Chicago Press, Chicago, pp. 55–77.

Hagfors, T., Nanni, B., and Stone, K.: 1968, *Rad. Sci.* **3**, 491–508.

Leadabrand, R. L., Dyce, R. B., Fredriksen, A., and Presnell, R. I.: 1960, *J. Geophys. Res.* **65**, 3071–3078.

Mulholland, J. D. and Block, N.: 1967, *JPL Lunar Ephemeris* Number 4, 1967, Technical Memorandum 33-346, Jet Propulsion Laboratory, Pasadena, California.

Pettengill, G. H.: 1960, *Proc. IRE* **48**, 933–934.

Pettengill, G. H. and Henry, J. C.: 1962, **67**, 4881–4885.

Pettengill, G. H. and Thompson, T. W.: 1968, *Icarus* **8**, 457–471.

Thompson, T. W.: 1971, *Icarus* **13**, 363–370.

Thomson, J. H. and Ponsonby, J. E. B.: 1968, *Proc. Roy. Soc. London* **A303**, 477–491.

Thompson, T. W. and Zisk, S. H.: 1972 Chapter 1C in *Thermal Characteristics of the Moon*, Vol. 28 of *Progress in Aeronautics and Astronautics*, MIT Press, Cambridge, Mass., pp. 83–117.

United States Naval Observatory: 1965, *The American Ephemeris and Nautical Almanac*, U.S. Government Printing Office, Washington, D. C.

HIGH-RESOLUTION RADAR MAPS OF THE LUNAR SURFACE AT 3.8-cm WAVELENGTH

S. H. ZISK, G. H. PETTENGILL,* and G. W. CATUNA

Haystack Observatory, Massachusetts Institute of Technology, Westford, Mass., U.S.A.

(Received 30 June, 1973)

Abstract. The entire earth-facing lunar surface has been mapped at a resolution of 2 km using the 3.8-cm radar of Haystack Observatory. The observations yield the distribution of relative radar backscattering efficiency with an accuracy of about 10% for both the polarized (primarily quasi-specular or coherent) and depolarized (diffuse or incoherent) scattered components. The results show a variety of discrete radar features, many of which are correlated with craters or other features of optical photographs. Particular interest, however, attaches to those features with substantially different radio and optical contrasts. An anomaly near 63° is noted in the mean angular scattering law obtained from a summary of the radar data.

1. Introduction

Observations of the Moon by radar over the past two decades have produced much information on the average backscattering properties of the lunar surface over a wide range of wavelengths. The observed distribution of echo power with delay and/or doppler frequency has been interpreted as caused by reflections from a relatively smooth, undulating surface, with the shape of the distribution determined by the average slope of this surface**. In addition to this coherent, quasi-specular component, an incoherent, largely unpolarized diffuse component is seen in the echoes originating some distance from the center of the disk and has been interpreted as originating in wavelength-sized structure, primarily associated with rocks on or near the surface. This interpretation has been strengthened by the discovery of anomalously enhanced, incoherent radar echoes from the region of the crater Tycho (Pettengill and Thompson, 1968), a crater known to be bright on optical photographs, to possess an extensive system of surface rays, and to display a strong thermal enhancement under eclipse conditions.

The first article in this series (I) discussed the general method of high-resolution measurements of the radar backscatter from the lunar surface (Pettengill *et al.*, 1973). Article II (Thompson, 1973) contains the results of such a set of measurements at a wavelength of 70 cm. In this article (III), we present a set of measurements at 3.8-cm wavelength. At this wavelength we expect to be sensitive to roughness at a scale of from 1 to 50 cm, as compared to a scale of 20 to 1000 cm at 70-cm wavelength. A comparison of the data at the two wavelengths with each other and with optical photographs and other data yields clues to the age and history of many features of the

* Now at Department of Earth and Planetary Sciences, M.I.T.

** See Evans and Hagfors (1971) for an excellent review and bibliography.

The Moon **10** (1974) 17–50.